Influence of Bond Kinematics on the Rupture of Non-Chiral CNTs under Stretching–Twisting

Bruno Faria, Nuno Silvestre and José N. Canongia Lopes

Abstract This chapter focuses on the role played by bond kinematics in the collapse behaviour of armchair and zig-zag CNTs under combined stretching-twisting. The analyses are performed through MD simulations, using LAMMPS code with the built-in potential AIREBO for C–C bonds. Incremental combinations of stretching displacements and twisting rotations are imposed to the CNT end atoms. The results are first analyzed in the form of diagrams of energy at rupture versus the twisting-to-stretching rate and diagrams of interaction between the axial stretching displacement at rupture and the angle of twist at rupture. A detailed study on the variation of bond length and angle amplitude with the imposed stretching and twisting deformations is shown. The case of pure stretching is first described, as a reference case. Two combined twisting-stretching cases and the pure twisting case are dealt with separately for zig-zag and armchair CNTs. It is concluded that two kinematic mechanisms influence the rupture of CNTs: one is the bond elongation for low twisting-to-stretching rate and other is the hexagonal cell distortion for moderate to high twisting-to-stretching rate.

Keywords Carbon nanotube · Tension · Torsion · Collapse · Kinematics

B. Faria
Department of Civil Engineering and Architecture, ICIST, Instituto Superior Tùcnico, University of Lisbon, Av. Rovisco Pais 1049-001 Lisboa, Portugal
e-mail: bmsfaria@gmail.com

J. N. C. Lopes
Department of Chemical and Biological Engineering, CQE, Instituto Superior Tùcnico, University of Lisbon, Av. Rovisco Pais 1049-001 Lisboa, Portugal
e-mail: jnlopes@ist.utl.pt

N. Silvestre (✉)
Department of Mechanical Engineering, IDMEC, Instituto Superior Tùcnico, University of Lisbon, Av. Rovisco Pais 1049-001 Lisboa, Portugal
e-mail: nsilvestre@ist.utl.pt

K. I. Tserpes and N. Silvestre (eds.), *Modeling of Carbon Nanotubes, Graphene and their Composites*, Springer Series in Materials Science 188,
DOI: 10.1007/978-3-319-01201-8_9,

1 Introduction

Carbon nanotubes (CNTs) are known for their unique mechanical, thermal and electrical properties. In the past two decades these properties were extensively studied with promising results (Wang and Liew 2008; Wang et al. 2010; Wernik and Meguid 2010; Byrne et al. 2010; Zhao and Luo 2011). The potential application of CNTs as basic elements in nano-devices such as nano-drive systems, nano-actuators or nano-oscillators, for instance as spring elements in torsional paddle oscillators or twisting bearings in nano-electric motors, prompted research on CNT mechanical behaviour under different directional loads (Williams et al. 2002; Fennimore et al. 2003; Hall et al. 2012). The research on the stiffness and strength of CNTs under different loading can be accomplished with either experiments or molecular dynamics (MD) simulations. Owing to the complexity in setting up rigorous test arrangements to make measurements at the nanoscale, experimental investigations are scarce (Hall et al. 2006, 2010; Xu et al. 2009; Sun et al. 2012). On the other hand, MD simulations have been widely used to study the mechanical behaviour of CNTs. Both the pure axial (tensile and compressive) and the pure twisting mechanical behaviours of armchair, zigzag and chiral CNTs were investigated (Yakobson et al. 1996; Sears and Batra 2004; Bao et al. 2004; Tserpes et al. 2006; Batra and Sears 2007; Chang 2007; Agrawal et al. 2008; Georgantzinos and Anifantis 2009; Arash and Wang 2012; Shima 2012). However, pure loading actions are difficult to occur at nanoscale level due to support imperfections, load eccentricities and geometrical inaccuracies of fixing CNTs in nano-devices. Thus, combinations of individual (pure) loadings are expected to occur. Understanding the CNTs mechanical response to combined loading is crucial to the design and optimization of CNT-based devices.

Regarding the use of MD to simulate CNTs under combined twisting-stretching, few works have been published (Jeong et al. 2007a, b; Talukdar and Mitra 2010). Jeong et al. (2007a) concluded that armchair and zig-zag CNTs under combined tension-twisting have decreasing tensile strength with linearly increasing twist. Talukdar and Mitra (2010) concluded that the defects change significantly the mechanical properties of armchair CNTs as well as their failure stresses and failure strains. Jeong et al. (2007b) developed failure criteria for the strength of armchair CNTs under tension-twisting and indicated that yielding or fracture behaviour of CNTs "*should be described by detailed atomistic observations involving chemical bond breaking, and therefore cannot be described with only macroscopic or continuum modeling that lack these atomistic details*". This is the main reason for using MD simulations in the present study, instead of either molecular mechanics or continuum models. In recent papers, Faria et al. (2013a, b) studied the twist-induced elastic anisotropic behaviour of chiral CNTs under pure twisting and moderate-to-high twist-to-stretching rates, as well as their stifness, strength and fracture toughness. We showed that the addition of axial tension (stretching) plays a key role in the chiral CNT linear and post-buckling stiffness. We also studied the continuous evolution of (i) chiral CNTs strength and fracture

toughness and (ii) the type of failure mechanism, under different twist-tension rate regimes (either low, moderate or high).

In this chapter, a study on the influence of bond kinematics and hexagonal lattice deformation on the CNTs mechanical behaviour is performed, in particular their rupture (1st failure). With this purpose, zig-zag and armchair CNTs are selected since the bond kinematics of chiral CNTs have already been investigated by Faria et al. (2013a, b). The CNT is subjected to tensile and torsional loads by imposing specific combinations of stretching and twisting displacements to the CNT boundary atoms. Using LAMMPS classical molecular dynamics simulator (Plimpton 1995), the carbon–carbon interaction parameters are modelled by the latest version of the AIREBO potential proposed by Stuart et al. (2000) and based on the well-known Brenner's second generation bond order potential. Bond lengths and angle amplitudes were measured after each simulation using the tools built-in VMD visualization software.

2 Molecular Dynamics Simulation

Molecular dynamics (MD) simulations were performed using the Large Scale Atomic/Molecular Massively Parallel Simulator (LAMMPS) (Plimpton 1995). The Adaptive Intermolecular Reactive Empirical Bond Order Potential (AIREBO), included in the LAMMPS software package, was used to model the inter-atomic forces present in the covalent binding of carbon in the CNT structure. The AIREBO potential is an improved version of Brenner's well-known second generation Reactive Empirical Bond Order Potential (REBO) that includes a Lenhard-Jones potential form to describe the Van-der-Waals long-range interactions and a torsional term for the σ-bond torsion. The general form of the AIREBO potential is

$$E = \frac{1}{2}\sum_i \sum_{j\neq i} \left[E_{ij}^{REBO} + \sum_{k\neq i,j} \sum_{l\neq i,j,k} E_{k,i,j,l}^{Tors} + E_{i,j}^{LJ} \right] \quad (1)$$

More detailed expressions can be found in Stuart et al. (2000). For a given CNT with radius R and length L, both end sections are located at $x = \pm L/2$ (x is the tube axis). For pure tensile loads, incremental axial displacements are imposed in opposite directions, $u = -0.025$ Å for atoms located at $x = -L/2$ and $u = +0.025$ Å for atoms at located $x = +L/2$. These imposed displacements stretch the CNT by 0.050 Å in each increment. For pure torsional loads, a twisting deformation is imposed to the atoms located in both ends of the CNT. The end sections rotate an angle ϕ about the x axis in opposite directions. The rotation angle per simulation is $\phi = +0.5° = +\pi/360°$ rad for the atoms at located $x = -L/2$ and $\phi = -0.5° = -\pi/360°$ rad for the atoms located at $x = +L/2$. With these rotations imposed to the CNT boundary atoms, the CNT twists by $\Delta\phi_0 = 1.0° = \pi/180°$ rad. During the simulation the CNT is allowed to relax, reaching a new equilibrium state while maintaining the prescribed displacement and rotation. The "0" subscripts mean either "pure stretching" (no twisting) or "pure twisting" (no stretching). In

order to impose combinations between tensile and twisting deformations, the following relationship is adopted between the combined Δu and $\Delta\phi$,

$$\left(\frac{\Delta u}{\Delta u_0}\right)^2+\left(\frac{\Delta \phi}{\Delta \phi_0}\right)^2=1 \tag{2}$$

$$\Delta u=\Delta u_0 \cos\beta, \quad \Delta\phi=\Delta\phi_0 \sin\beta \tag{3}$$

where the parameter β varies from 0 to 90°, as depicted in Fig. 1a. For $\beta = 0^\circ$, it is obtained $\Delta u = \Delta u_0$ and $\Delta\phi = 0$, i.e., pure stretching behaviour (no twisting). For $\beta = 90°$, it is obtained $\Delta\phi = \Delta\phi_0$ and $\Delta u = 0$, i.e., pure twisting behaviour (no stretching). Table 1 shows the correspondence between the angle β and the twisting-to-stretching rate ϕ/u.

All simulations were performed at a temperature of 300 K using the canonical NVT ensemble and Nose–Hoover thermostat. The newtonian equations of motion were integrated using the velocity-Verlet algorithm. A timestep of 0.8 fs was used and all simulations comprised 10,000 time-steps. The configurational (or strain) energy V of the CNT calculated in the end of each simulation corresponds to the average value of the energy within the last 4,000 time-steps. Four-hundred simulations were performed for each β, in the case of pure stretching ($\beta = 0°$), combined stretching-twisting and pure twisting ($\beta = 90°$). In order to study the mechanical behaviour of CNTs under pure and combined tensile and torsional loads, we have considered the following zig-zag and armchair CNT structures[1]:

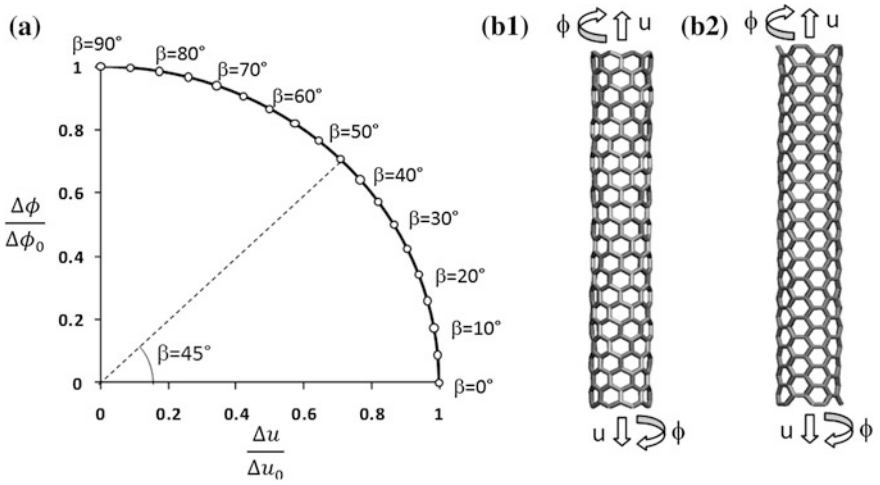

Fig. 1 **a** Stretching-twisting combinations, **b** zig-zag (8, 0) CNT, **c** armchair (5, 5) CNT

[1] The chiral vector (n, m) represents the way grapheme sheet is wrapped. The pair of indices n and m denote the number of unit vectors along two directions in the honeycomb crystal lattice of graphene. If $m = 0$, the CNTs are called zig-zag. If $n = m$, the CNTs are called armchair. If $m \neq 0$ and $m \neq n$, the CNTs are called chiral.

Table 1 Correspondence between angle β and the twisting-to-stretching rate ϕ/u

β																		
0°	5°	10°	15°	20°	25°	30°	35°	40°	45°	50°	55°	60°	65°	70°	75°	80°	85°	90°
ϕ/u (rad/Å)																		
0	0.03	0.06	0.09	0.13	0.16	0.20	0.24	0.29	0.35	0.42	0.50	0.60	0.75	0.96	1.30	1.98	3.99	∞

zig-zag (8, 0) with L = 46.3 Å and R = 3.1 Å, having an aspect ratio L/D = 7.4 and 352 atoms; armchair (5, 5) with L = 47.3 Å and R = 3.4 Å, having an aspect ratio L/D = 7.0 and 380 atoms. These are depicted in Fig. 1b, c. A similar study was performed by the authors for the case of chiral CNTs. The interested reader is referred to Faria et al. (2013a, b). The MD simulation results concerning the zig-zag and armchair CNTS are presented and discussed in the following sections.

3 Interaction Diagrams

MD simulations were performed on the CNTs (5, 5) and (8, 0), for pure stretching, combined stretching-twisting and pure twisting. This was achieved by adopting the relation defined in Eq. (2). Results were obtained for β from 0 (pure stretching) to 90° (pure twisting) using a stepwise increase of 5°. The results shown in Fig. 2 depict the variation of the deformation energy per atom, V, as a function of the angle of twist per length, $\alpha = \phi/\mathrm{L}$, for both CNTs.

Figure 2 shows clear differences between both CNTs in terms of energy of deformation achieved at rupture—here, "rupture" means the equilibrium state of the CNT at which the first failure of a C–C bond is reached. For pure stretching ($\beta = 0°$), the armchair tube reaches a higher energy of deformation (more than twice) of that of the zig-zag tube. This difference persists even in combined behaviour, as the twisting increases from $\beta = 5$ to 15°. For $\beta = 20°$ (twisting-to-stretching rate of 0.12 rad/Å) the deformation energy sharply drops to almost half, indicating the beginning of the twisting effects over the stretching ones. From then on, the deformation energy steadily decreases for increasing β and it seems to be more or less stabilized for $\beta \geq 50°$. It is also clear from Fig. 2a that the $V(\alpha)$ curves become less steep with increasing β, clearly showing that the deformation energy derives mainly from stretching the CNT rather than twisting it. Figure 2b differs significantly from Fig. 2a. In fact, the structural rupture takes place at a lower deformation energy for the zig-zag CNT when pure stretching ($\beta = 0°$) is involved, comparing to the armchair tube. However, as the twisting-to-stretching rate increases we see that the rupture deformation energy does not change much, implying that twisting does not affect the CNT rupture, which seems to be only affected by stretching. For $\beta = 45°$ (twisting-to-stretching rate of 0.35 rad/Å—Table 1), we see a small drop in the deformation energy. From $\beta = 45$ to 90°, previous trend is resumed and a steady slight increase in the rupture deformation energy occurs.

Note that, for the armchair CNT, the rupture points do not always correspond to the maximum energy achieved (remind that rupture is defined as the breaking of the first bond). This means that even when bonds break and 7–5 Stone-Waals defects start to appear the structure does not immediately break apart, but the CNT continues to stretch, reaching higher deformation energies and showing some resilience. This is seen mainly after $\beta > 30°$. On the other hand, zig-zag shows the

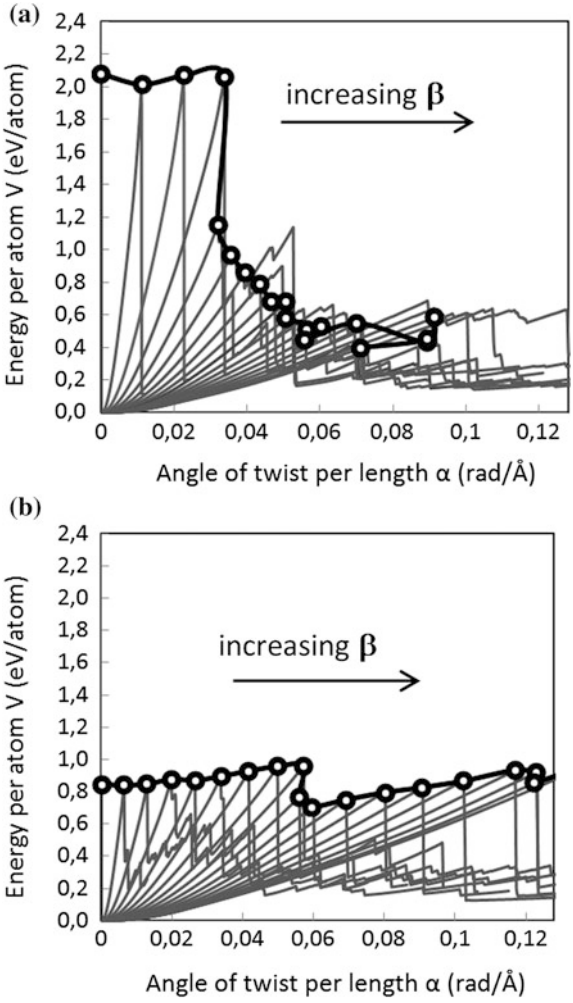

Fig. 2 Variation of the deformation energy, V, with angle of twist per length, α, for different values of β (rupture points are denoted by *circles*): **a** CNT (5, 5), **b** CNT (8, 0)

opposite behaviour. As soon as the first bond breaks, energy starts to sharply decrease, meaning that the structure collapsed or that it triggered a wide rupture.

Diagrams of interaction between the axial stretching u and the angle of twist ϕ at rupture are shown in Fig. 3a, b for the zig-zag and armchair CNTs, respectively. The (8, 0) zig-zag tube (Fig. 3a) has a maximum stretching displacement of roughly 10.0 Å if no twisting is applied. This CNT is able to augment its length from L = 46.3 to 56.3 Å without breaking. Furthermore, it is capable of maintaining the critical length of nearly 55–56 Å for low twisting-to-stretching rates (up to 0.29 rad/Å, i.e. $\beta = 40°$—see Table 1), denoting a clear non dependence on the twisting-to-stretching rate. A significant drop in u occurs for $\beta = 45°$, from 10 to 6.62 Å, which seems to indicate a clear interference of twist on the rupture

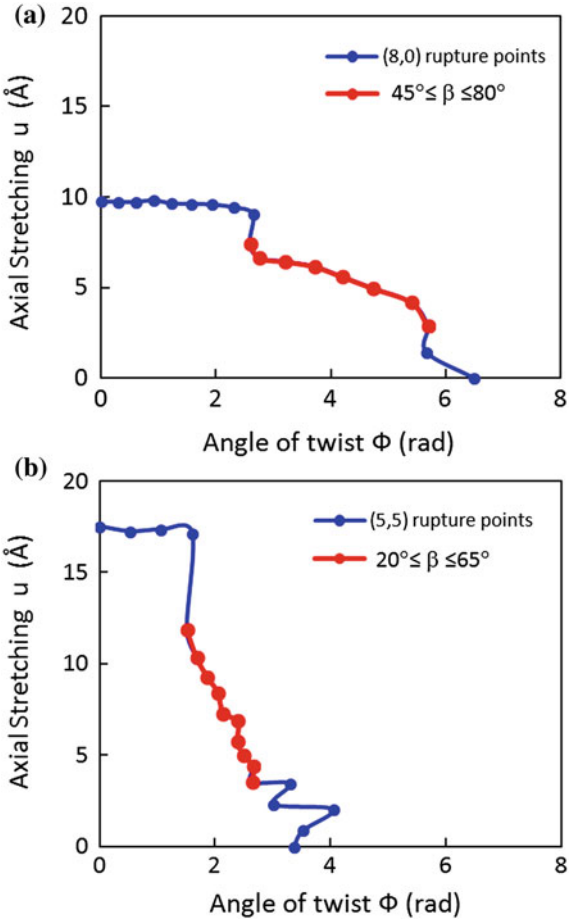

Fig. 3 Interaction diagrams between the axial stretching u (Å) and angle of twist ϕ (rad) for **a** zig-zag (8, 0) CNT and **b** armchair (5, 5) CNT

process. Increasing twisting-to-stretching rates (from $\beta = 45$ to 80°), denoted in Fig. 3a by the red dots and lines, imply a steady (almost linear) reduction of the maximum axial stretching, which is reduced to 2.88 Å for $\beta = 80°$. This means more or less 0.1 Å reduction per 5° increase in β. Pure twisting ($\beta = 90°$) induces rupture at an angle of twist of 6.5 rad (slightly more than a full 2π turn). Comparing Figs. 2b and 3a it can be concluded that although the deformation energy is derived mainly from bond stretching, the fact that the decrease in axial stretching from $\beta = 45$ to 80° is opposing a slight increase in deformation energy suggests that twisted CNTs can also increase their potential energy due to bond angle variation.

The armchair (5, 5) interaction diagram is shown in Fig. 3b. In pure stretching, the armchair CNT extends 17.5 Å without rupture. This means that the armchair CNT length increases from L = 47.3 to 64.8 Å without breaking. But when combined torsional-tensile displacements are applied, the armchair CNT can keep

this length only to a twisting-to-stretching rate of 0.10 rad/Å ($\beta = 15°$—see Table 1). If a twisting-to-stretching rate of 0.12 rad/Å is applied, the maximum stretching length is reduced 32 %, indicating that this twisting-to-stretching rate forces the CNT to break apart sooner than expected. After this major drop, the axial stretching at rupture continues to drop in an almost linear trend. This stage steeply descendent branch of the interaction curve is shown in Fig. 3b. For $\beta \geq 65°$, there is no clear trend besides a clear drop in axial stretching maximum length.

For pure loading, some differences between the two CNTs deserve to be mentioned, namely that:

- the armchair CNT reaches almost twice the maximum elongation achieved by the zig-zag CNT: $u = 17.5$ Å for the armchair CNT and $u = 10.0$ Å for the zig-zag CNT. The armchair CNT resists much better (without bond break) to pure stretching than the zig-zag CNT.
- the zig-zag CNT reaches almost twice the maximum twist achieved by the armchair CNT: $\phi = 6.5$ rad for the zig-zag CNT and $\phi = 3.36$ rad for the armchair CNT. The zig-zag CNT resist much better (without bond break) to pure twisting than the armchair CNT.

For combined stretching-twisting loading, it is concluded that interaction diagrams involve two different branches:

- For low twisting-to-stretching rate, a horizontal branch exists in which the axial stretching does not vary much with the low amount of twist. The width of this branch is distinct for armchair and zig-zag CNTs. The zig-zag CNT withstands combined stretching-twisting to a higher extent than the armchair CNT: this corresponds to $\beta = 40^{\circ}$ for zig-zag CNT and $\beta = 15^{\circ}$ for the armchair CNT.
- For moderate to high twisting-to-stretching rate, an almost (with some scatter) linear descending branch exists in both interaction u-ϕ diagrams. This "linear" branch is much steepest for the armchair CNT than for the zig-zag CNT, which means that the strength of the armchair CNT is much more affected by the twisting-to-stretching rate than the zig-zag one.

4 Bond Kinematics

The interaction diagrams corresponding to CNT rupture (1st bond failure) presented in the previous section state that both (5, 5) and (8, 0) CNTs break apart for distinct maximum stretching displacements and strains. Furthermore, if twisting deformations are imposed in combination with stretching deformations, both CNTs behave differently in order to accommodate these deformations. As a consequence, their rupture behaviour follows dissimilar trends. Albeit rupture can be seen as a global phenomenon, it may depend on CNT diameter and length. In the cases studied herein, these two variables are made very similar. Thus, the major factor contributing to that dissimilar behaviour is chirality. In order to

understand why CNT rupture occurs at different stretching displacements and different twisting angles, it is mandatory to assess how the hexagonal lattice of armchair and zig-zag configurations accommodates the imposed deformations. To achieve this goal, the kinematics of the hexagonal lattice is analyzed, which comprises the assessment of bond length variations and angle amplitude variations with the prescribed displacements. For both CNTs the hexagonal cell in which rupture first occurs is selected and the bond length and angle variations are measured against the initial equilibrium values, i.e. before any displacements are imposed. Figure 4a presents a scheme with (i) the bond labels x, y and z and (ii) the angle labels a, b and c. Figure 4b depicts both CNTs in initial equilibrium state and fully tensioned state.

In the following sections, results regarding bond length variations and angle amplitude variations are presented. Firstly, pure stretching is established as the reference case. The results for combined stretching-twisting deformations (including pure twisting) are then presented and compared with the reference case, i.e. pure stretching deformations.

4.1 Pure Tensile Behaviour

Figure 5a gives clear evidence that bonds **y** and **z** are responsible for the high stretching displacement (17.5 Å) and high strain ($\varepsilon = 17.5/47.3 = 37$ %) achieved by (5, 5) CNT before rupture is attained. As the stretching deformation is imposed to the (5, 5) CNT, bonds **y** and **z** increase their length simultaneously and with equal variation ($\sim$23 %), meaning that they give equivalent response to the deformation imposed.

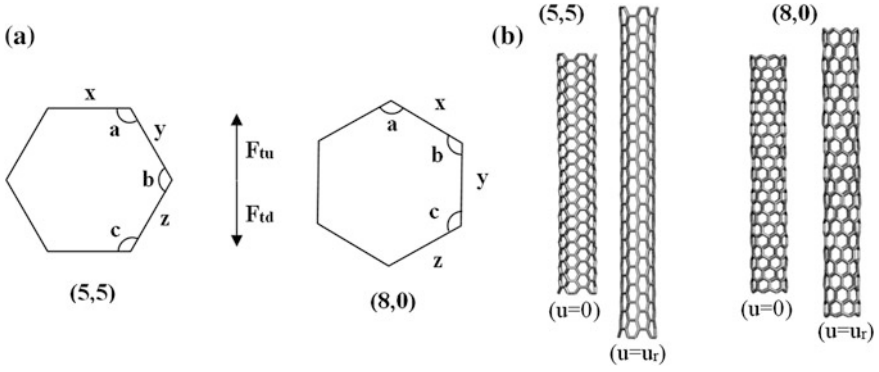

Fig. 4 **a** Scheme representing the adopted nomenclature. In this scheme, the *hexagon* cells are aligned with the tube axis, for which the tensile loads, F_{tu} and F_{td}, are applied. x, y and z represent bonds while a, b and c represent angles. **b** Representation of the two CNTs, each one with two representations, the initial equilibrium state (*left*) and the pre-rupture state for pure stretching (*right*)

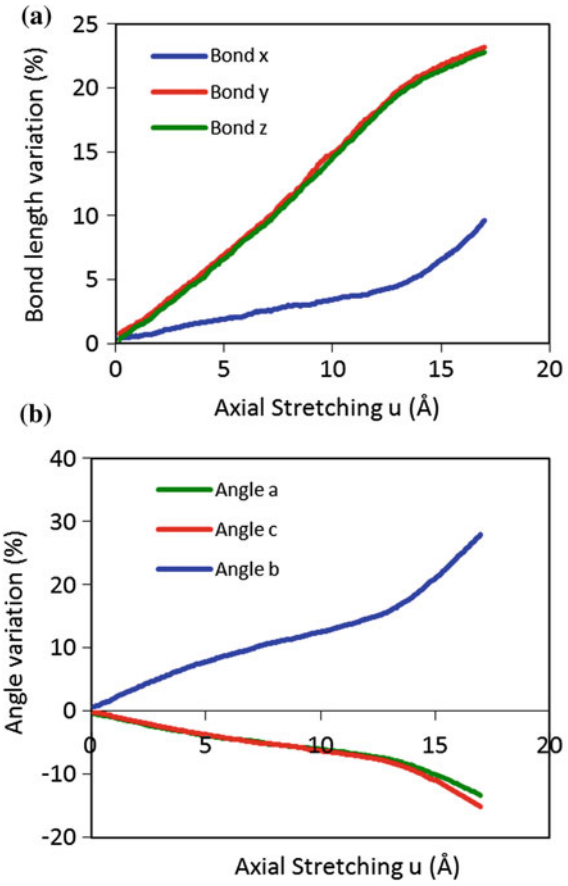

Fig. 5 CNT (5, 5): Variation, with the axial stretching u (Å), of **a** bond length variation and **b** angle amplitude variation

Bond **x**, positioned transversally to the tube axis (see Fig. 4a), also presents some positive length variation (increase of $\sim$10 %) but to a lesser extent than the other two bonds. The axial stretching imposed to the (5, 5) CNT also implies a $\sim$28 % increase of amplitude of angle **b,** forcing angles **a** and **c** to close (see Fig. 4b). For a stretching displacement up to 13.0 Å, there is a linear trend between the bond variation and the imposed axial stretching u (Fig. 4a). Similar linear trend also exists for between the angle variation and imposed axial stretching u (Fig. 4b). For stretching displacement greater than 13.0 Å, there is a clear change of the curves' slopes. The data suggests that around $u = 13.0$ Å both bonds **y** and **z** reach their maximum length. In order to accommodate further stretching without rupture, the hexagonal lattice starts to open angle **b** at a faster rate: it rapidly increases from 15 % variation at $u = 13.0$ Å to 28 % variation at $u = 17.5$ Å. Consequently, bond **x** has to increase faster also. If these changes are uniform throughout the CNT structure, it is expected that a diameter reduction occurs because bond **x** increase of 10 % variation cannot compensate a 28 % variation of angle **b**.

Figure 7 depicts the variation of diameter reduction with u, for the (5, 5) CNT. The red curve shown in Fig. 7 proves that assumption. It is clear that a 2 % reduction of CNT diameter is achieved for $u < 13.0$ Å. But for $u > 13.0$ Å, the curve slope increases and the diameter reduction rapidly achieves 7 %, which is a rather significant value since the CNT diameter decreases about 0.5 Å.

The (8, 0) CNT behaves very differently because it has a bond that is perfectly aligned with the direction in which the stretching is imposed. That is bond **y**. As we can see in Fig. 6a, bond **y** increases its length up to 21 % of its initial value and then breaks, inducing the CNT global failure. Bonds **x** and **z** show minor variations of about 6 % and are not so affected as bond **y**, mostly because their initial directions are far from the axial direction, although their are not fully orthogonal either. Angle **a** decreases its amplitude as a consequence of being pulled, forcing a small increase in the amplitudes of angles **b** and **c**. Notice that the same phenomenon found in (5, 5) CNT is also present to a lesser extent in (8, 0) CNT. From $u = 7.0$ to 9.75 Å, there is a sudden decrease of the amplitude of angle **a** (the slope

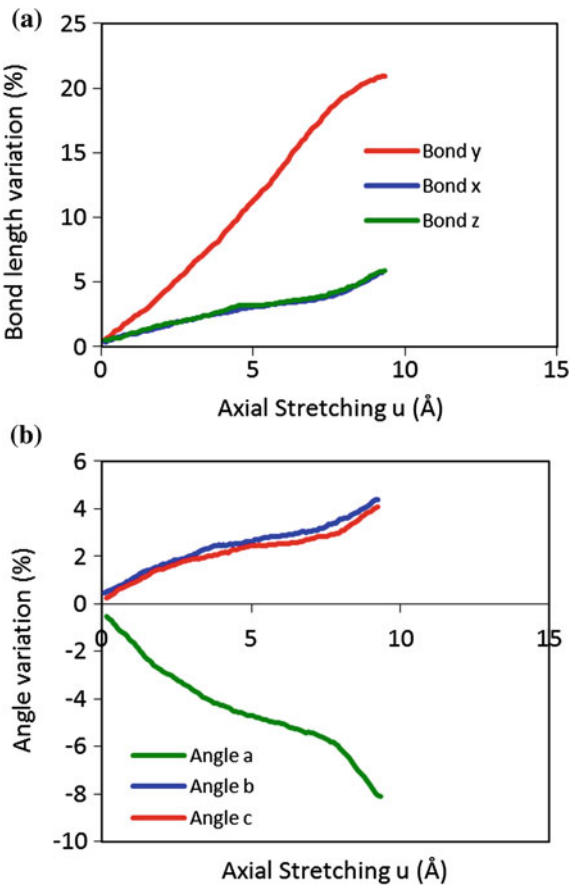

Fig. 6 CNT (8, 0): Variation, with the axial stretching u (Å), of **a** bond length variation and **b** angle amplitude variation

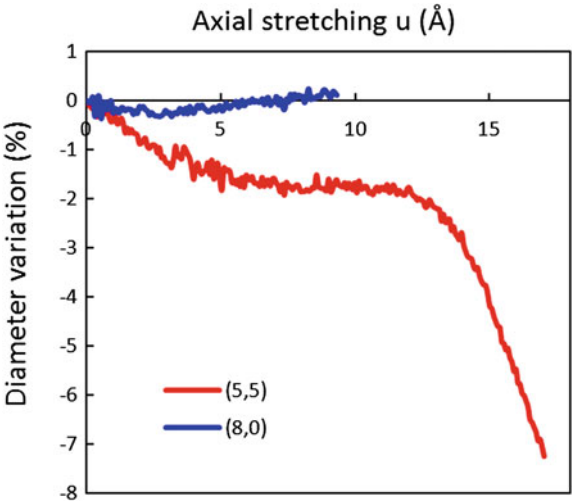

Fig. 7 Variation, with the axial stretching u (Å), of diameter variation

of angle **a** is the steepest in Fig. 6b. This enforces some increase in the amplitudes of angles **c** and **b**, but not very prominent variations of length of bonds **x** and **z**. Thus, some diameter reduction would be expected. However, the opposite scenario is obtained, as depicted in Fig. 7, in which there is a slight increase of CNT diameter.

In fact, a decrease of (8, 0) CNT diameter really happens, as we can see from Fig. 8. However, this diameter decrease is purely local and is localized in the CNT

Fig. 8 Localised diameter reduction in the region where the CNT (8, 0) rupture occurs

section where rupture will then occur. This diameter reduction is not reflected in the blue curve of Fig. 7 because the diameter variation depicted in this figure is the average value measured in several cross-sections of the CNT, in a given instant. The reason why the diameter reduction has a global nature in armchair CNTs and local nature in zig-zag CNTs is not clear. Yet, we suggest that it is a consequence of the process of axial load transfer throughout the whole CNT. If we notice Fig. 4b, the (5, 5) CNT lattice orientation is such that only bonds **y** and **z** have projection in the axial direction (x is orthogonal to it) but are not fully aligned to it. The **y** and **z** bonds form a "zig-zag" chain along the axial direction that behaves like an elastic spring and enhances the axial load transfer. This is the reason behind the very high failure strain of (5, 5) CNT, reaching 37 %! In case of (8, 0) CNT, **x** and **z** bonds are almost perpendicular to the axial direction and bond **y** is the one that is mostly responsible for the CNT elongation. The "armchair" chain formed by **y** and **x** (or **z**) bonds is less flexible and the load transfer between bonds **y** and **x** (or **z**) is harder to achieve, giving rise to local necking phenomena.

4.2 Twisting and Combined Stretching-Twisting Behaviour

In this section, it is considered the behaviour of the CNTs under combined stretching-twisting and pure twisting. Three β values are considered (see Fig. 1a):

- $\beta = 45°$ corresponding to a twisting-to-stretching rate ϕ/u = 0.35 rad/Å (Table 1). It means that the CNT is twisted 0.35 radians for each angstrom that it is stretched.
- $\beta = 60°$ corresponding to a twisting-to-stretching rate ϕ/u = 0.60 rad/Å (Table 1). This means that, for each angstrom of stretching displacement, the CNT is twisted 0.60 rad.
- $\beta = 90°$ corresponding to a twisting-to-stretching rate ϕ/u = ∞ (Table 1) or a stretching-to-twisting rate u/ϕ = 0. It means that the CNT is not stretched but only twisted. This situation corresponds to pure twisting.

4.2.1 Armchair CNT

For the (5, 5) CNT, Figs. 9 and 10 depict the bond length variations and angle amplitude variations with respect to the angle of twist ϕ, respectively. Each curve corresponds to a given β value and to a given ϕ/u rate. Thus, and given a ϕ value, it is always possible to obtain the u value using one of the adopted ϕ/u rates. From Fig. 3b and for these β values (45 and 60°), it becomes understandable that the rupture points are placed in the red region of the interaction diagram, for which rupture is mostly influenced by twisting. Figures 9 and 10 are easier to interpret if the CNT MD simulations are visualized while the ϕ/u rate is imposed to the CNT.

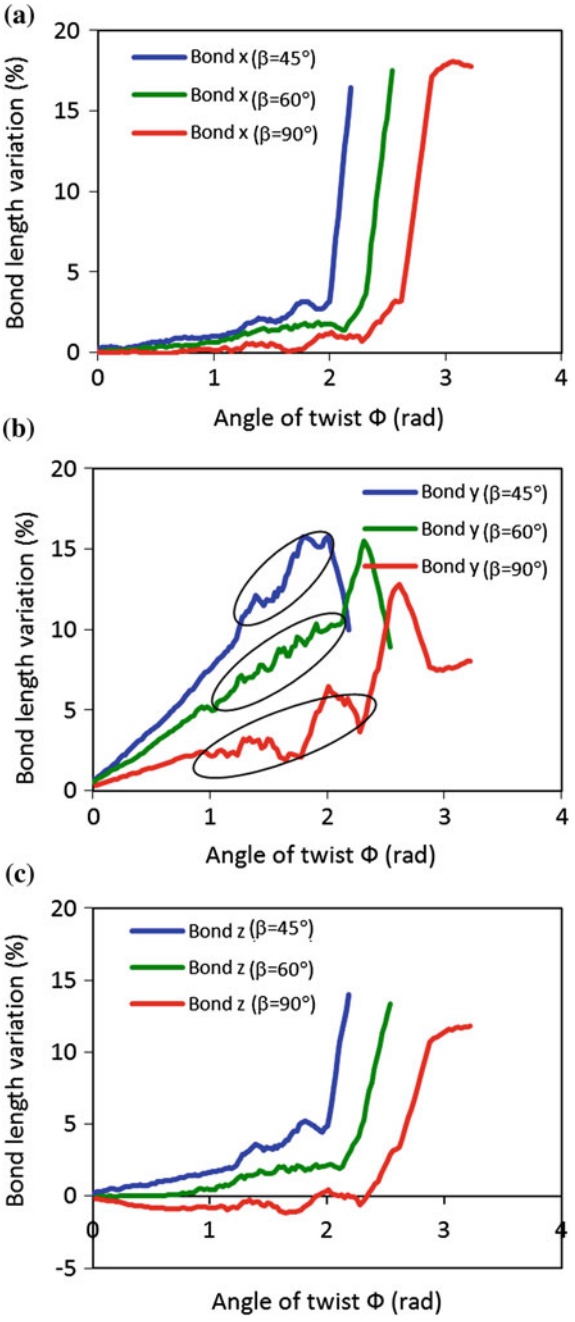

Fig. 9 CNT (5, 5): Variation, with the angle of twist ϕ (rad), of **a** bond x length variation, **b** bond y length variation, and **c** bond z length variation

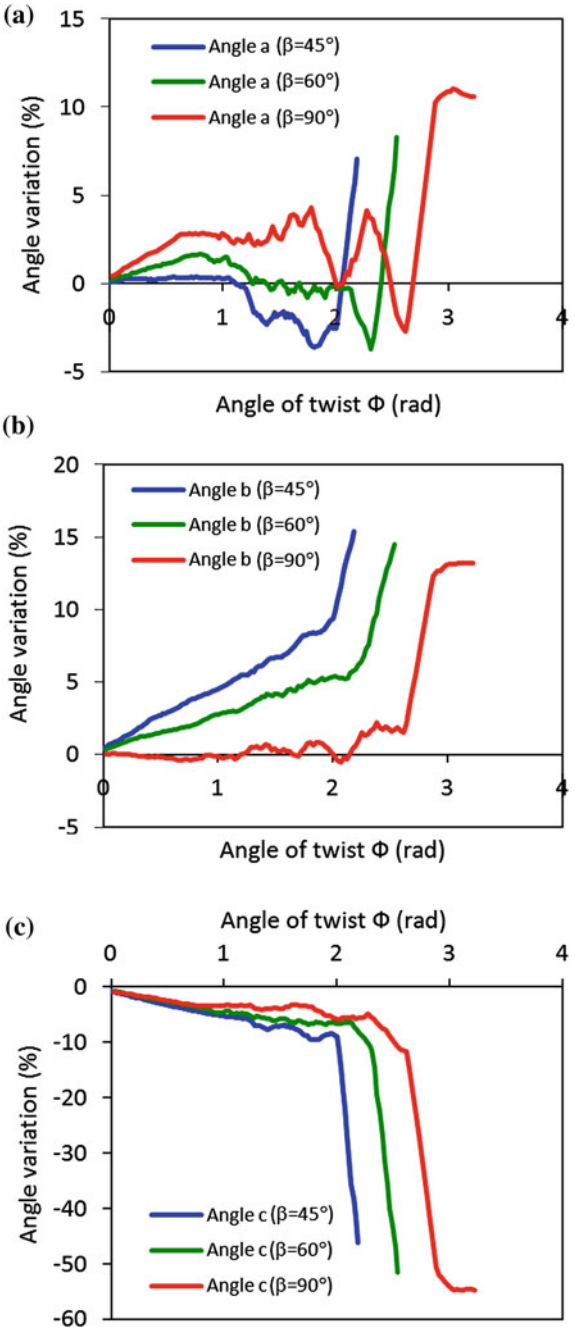

Fig. 10 CNT (5, 5): Variation, with the angle of twist ϕ (rad), of **a** angle *a* variation, **b** angle *b* variation, and **c** angle *c* variation

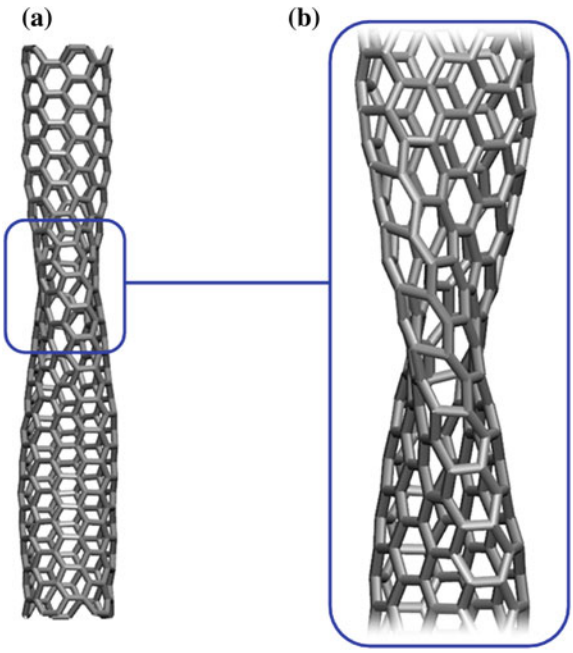

Fig. 11 CNT (5,5): **a** Visualization of the *helix shaped* configuration and **b** Zoom-in of the distorted *hexagonal* cells

Three different events might occur. Firstly, at a certain instant, the CNT buckles from a circular cylindrical shape into an oval helix shape, as depicted in Fig. 11a. This shape appears to rotate but, in fact, it's an illusion caused by the surface waves. This movement induces atomic oscillations in the radial direction. This helix shape configuration permits the CNT to relax local tensions arising from twisting. However, because part of the oval section surface is strongly curved, it also imposes local tensions in the mostly bent zones of CNT wall. As a result, bond lengths and angle amplitudes measured in a fixed hexagonal cell oscillate and the results show some scatter. The regions with oscillations due to the "rotating" helix shape are denoted in Fig. 9b. Secondly, and for a given ϕ value, the helix shape stops oscillating because the angle of twist and stretching displacement are high enough to stiffen the helix-shaped surfaces of the CNT. At this point, the CNT has two accentuated surface curvatures due the high ovalization. This gives rise to local tensions and impedes further oscillations. Beyond this stage, bond lengths and angle amplitude change rapidly as the CNT continues to twist. Thirdly, two regions of heavily distorted hexagonal cells are formed in the axial direction (Fig. 11b). These regions are situated in the mid section of the CNT. These hexagonal cells are forced to distort because of the torque. The twisting rotations imposed in opposite directions to the CNT top and bottom ends, tend to concentrate strain in its mid section, especially in the curved surfaces of the helix-shaped CNT. The increasing strains existing in hexagon cells require now the increase of bond lengths beyond the breaking instant.

Bond length variation can naturally be separated in three stages, considering the events just described. Bond **x** length variation depicted in Fig. 9a holds the same trend for the three β values. The length of bond **x** increases marginally, below 4 %, before reaching the stage in which the hexagonal cell is distorted. After that, it shows a very high length increase. The length increase in the first and second stages is small and almost inversely proportional to the twisting-to-stretching rate ϕ/u. For instance, it is seen that length increase is higher for $\beta = 45°$ (blue curve) than for $\beta = 90°$ (red curve). Although bond **x** does not show a variation exceeding 20 %, it is expected that this bond is responsible for the CNT rupture. We must be aware that a bond breaks for $\sim$23 % extension and that the bond length variation corresponds to average values. Thus, it is possible to have some bonds elongated by 23 % and still have average values below 20 %.

The length variation of bond **y** shows a higher increase than the other two bonds (**x** and **z**), during the first two stages and for the three β values considered. It is known that a continuum tube under torsion exhibits shear stresses in the contour direction (arising from torque) but also in the axial direction (arising from equilibrium). This shear stress state is characterized by principal stress directions oriented at 45° with respect to the contour and axial directions. These principal stresses correspond to tensile stresses in one direction but compressive stresses in the other (orthogonal) direction. Similar behaviour exists in CNT under twisting and the alignment of bond **y** is closer to the direction of tensile stresses. Therefore, the bond **y** increases its length the most. When the oscillations stop, increasing tensions stretch the bond even further, a fact that is visible for $\beta = 60°$ and $\beta = 90°$. The hexagonal cell distortions that follow relief this bond and decrease its length by closing angle **c** and opening angles **a** and **b** (see Fig. 11b).

Bond **z** (Fig. 9c) presents a length variation very close to that of bond **x**. Comparing the curves in Fig. 9c with the variations it showed when there was no twisting (Figs. 5b,6b), it is clear that the twisting direction misaligns the bond with the stretching direction. In fact, the bonds extend much less, even to $\beta = 45°$, showing poor load transfer. Once again, when severe deformation occurs in the hexagonal cell before rupture, the bond **z** (like bond **x**) increases its length.

Amplitude variations for angles **a, b** and **c** are shown in Fig. 10. Hexagonal cell deformation explains fairly well the very high slopes of the last portion of the curves. The hexagonal cell deformation consists mainly in the abrupt closing of angle **c.** As a consequence angles **b** and **a** have to open. This phenomenon occurs regardless of β value, and might indicate a possible cause for CNT rupture.

The amplitude variation of angles **b** and **c** is predictable. Angle **b** opens proportionally to the imposed stretching and inversely to the imposed twisting. Therefore, the curve slope is higher for lower β values. For $\beta = 90°$ (red curve), note that the variation of angle **b** is negligible while it is meaningful for $\beta = 45°$ (blue curve). On the other hand, angle **c** always closes: first because of stretching and then, for high twisting-to-stretching rates, because the twisting forces the amplitude to decrease. Angle **a** also exhibits these two opposed effects: stretching make it close while twisting make it open. For $\beta = 45°$, it is visible that these two effects cancelled each other prior to the CNT buckling into a helix shape tube.

Thus, angle **a** amplitude showed null variation. For $\beta = 60$ and 90°, it is clear that twisting component is predominant because the angle **a** opens. The oscillations of the helix shaped tube tend to close angle **a**. In fact, Fig. 10 shows that angle **a** closes in order to compensate an equal increase of angle **b** amplitude. Angle **a** amplitude variation also shows one negative peak for $\beta = 60°$ (green curve) and a positive peak beside two negative peaks for $\beta = 90°$ (red curve). These peaks are correlated with the length variation of bond **y** (Fig. 9b). Before cell distortion takes place, increasing local tensions tend to enlarge the length of bond **y** and force the closing of angle **a**. From the comparison between Figs. 9b and 10a, we see that the variations in these regions are complementary.

The rupture process can now be explained resorting to the observation of Fig. 12, which depicts the rupture mechanism and its sequence of steps. The last stage previously defined in curves shown in Figs. 9 and 10 was characterized by a severe distortion of the hexagonal cells situated in curved surface regions. This distortion was explained by the extreme closing of angle **c** and opening of angles **a** and **b,** while bond lengths abruptly increased. Rupture occurred at the end of this stage. Based on the visual representation of MD results, we suggest that rupture is triggered by the formation of a new bond, as depicted in Fig. 12, involving sp3 hybridization of the two carbon atoms that were brought into bond length distance by the closing of angle **c**. These two carbon atoms then return to sp2 hybridization due to the break of bond **z**, because this new state is energetically more favourable—recall that tension is released, not only by breaking of a tensioned bond but also by angular relaxation. This configuration originates a 7–5 Stone-Waals defect that spreads as the imposed stretching-twisting combination continues. Figure 12 shows this process for $\beta = 45°$. This failure mechanism was equally observed for all $\beta > 15°$, showing that rupture occurs in twisted (5, 5) CNTs in an identical process regardless of the twisting-to-stretching rate ($\beta > 15°$).

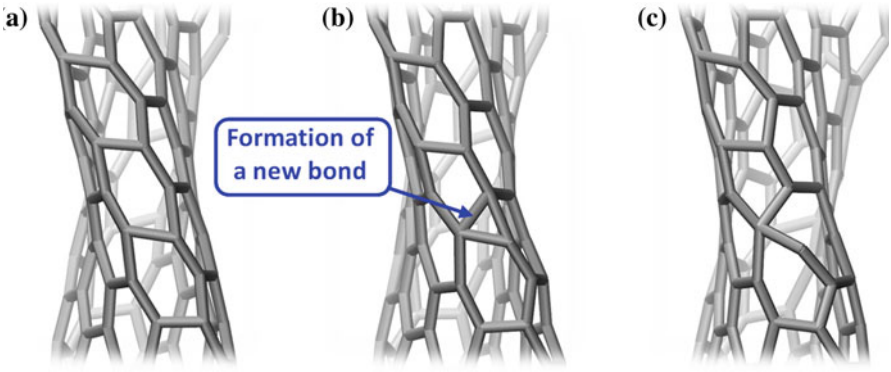

Fig. 12 (5, 5) CNT: sequential views showing the beginning of the rupture process for $\beta = 45°$

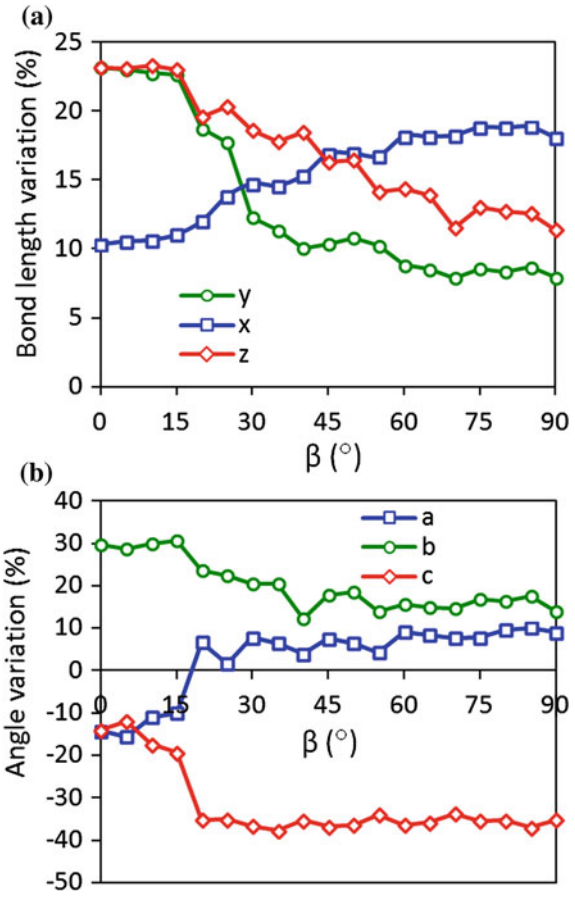

Fig. 13 CNT (5, 5): **a** bond length variation at rupture vs. β and **b** angle amplitude variation at rupture vs. β

Figure 13 depicts the variation, with β, of bond length and angle amplitude at rupture. These variables are scaled to their initial values and they correspond to the average value of the last 100 steps before rupture.

Firstly, it is seen that the influence of twisting-to-stretching rate ϕ/u (or β) on the kinematics of CNT rupture is relevant. The bond length increase remains almost unchanged from $\beta = 0$ to 15°. In this case, bonds **y** and **z** reach their maximum length ($\sim$23 %) and force bond **x** to stretch also. Angle **b** opens widely and obliges the other angles to decrease their amplitude. The CNT reaches its maximum length ($\sim$17.5 Å) for $0° \leq \beta \leq 15°$, meaning twisting effects are negligible in this range. CNT rupture is achieved by breaking of bonds **y** or **z**. From $\beta = 15$ to 20°, the angle amplitudes at rupture change a lot. The angle **b** amplitude drops but the angle still opens, while the amplitude of angle **a** is now positive (angle opens). The amplitude of angle **c** decreases the most and closes. For $\beta = 20°$, the amplitude of angles at rupture become characteristic of a distorted cell. From $\beta = 20$ to 90°, the amplitudes of the angles show some scatter but small

variation. In this range, the length of bond **y** shows a high decrease, bond **z** exhibits a smaller drop in its length, and bond **x** increases its length. However, none of these bonds achieve their maximum elongation ($\sim$23 %) in the range $20° \leq \beta \leq 90°$. Thus, we conclude that the rupture mechanism involves the deformation (distortion) of the hexagonal cell with abrupt closing of angle **c**. This leads to the formation of a new bond through sp3 hybridization of two carbon atoms, followed by breaking of a tensioned adjacent bond and new hybridization to sp2.

4.2.2 Zig-Zag CNT

The first fact to notice when comparing the (8, 0) CNT with (5, 5) CNT is that the former withstands much less axial stretching than the latter. Although it maintains similar axial stretching at failure in spite of increasing twisting-to-stretching rate, it also endures more twisting without rupture. The request is to explain the reason why it can endure more twisting when compared with (5, 5) CNT. The explanation clearly lies in the differences presented in the chiral matrix. Figures 14 and 15 depict the bond length variations and angle amplitude variations of (8, 0) CNT with respect to the angle of twist ϕ: recall the bond and angle nomenclature of (8, 0) CNT shown in Fig. 4a. The results shown in Fig. 6a (pure stretching) demonstrated that bond **y** length variation was responsible for much of the CNT elongation without rupture.

Firstly, let us discuss the $\beta = 45°$ case (blue curves in Fig. 14). We see that all bonds increase their length in a linear trend with the twist ϕ: bond **y** is the most elongated (achieving a maximum of 15.9 %) while the elongations of bonds **x** and **z** are fair and marginal, respectively. However, this linear path is abruptly changed for $\phi > 2.3$ rad as the length of bonds **x** and **z** increase sharply and the length bond **y** decreases steeply, indicating the occurrence of extreme deformation (distortion) of the hexagonal cell. This fact is confirmed by angle amplitude analysis (Fig. 15). Initially, there is a linear variation of all angles with the twist ϕ: angle **b** increases the most (achieving a maximum of 12.0 %) while the amplitudes of angles **a** and **c** decrease to a lesser extent.

As mentioned before, this linear path changes suddenly for $\phi > 2.3$ rad, and a sudden rise is observed in the amplitudes of angles **b** and **c** (Figs. 15b, c) while an abrupt decay of angle **a** occurs (Fig. 15a). This change of angle amplitudes is associated with a distortion of the hexagonal cell that leads to rupture, similarly to that observed for (5, 5) CNT—in this case, angle **a** closes instead. Notice that, for $\beta = 45°$, oscillations of helix shape rotations were not observed. Visual MD data confirms that a helix shape forms, similar to the one observed in Fig. 11a. From Fig. 3, we are able to mention that hexagonal cell distortion occurs in (8, 0) CNT for $\beta \geq 45°$ ($\phi = 2.6$ rad and u = 7.4 Å, Fig. 3a) while in (5, 5) CNT it takes place for $\beta \geq 20°$ ($\phi = 1.5$ rad and u = 11.9 Å, Fig. 3b). Comparing both CNTs, we see that (8, 0) CNT requires much larger twist ϕ and lower stretch u to collapse than the (5, 5) CNT.

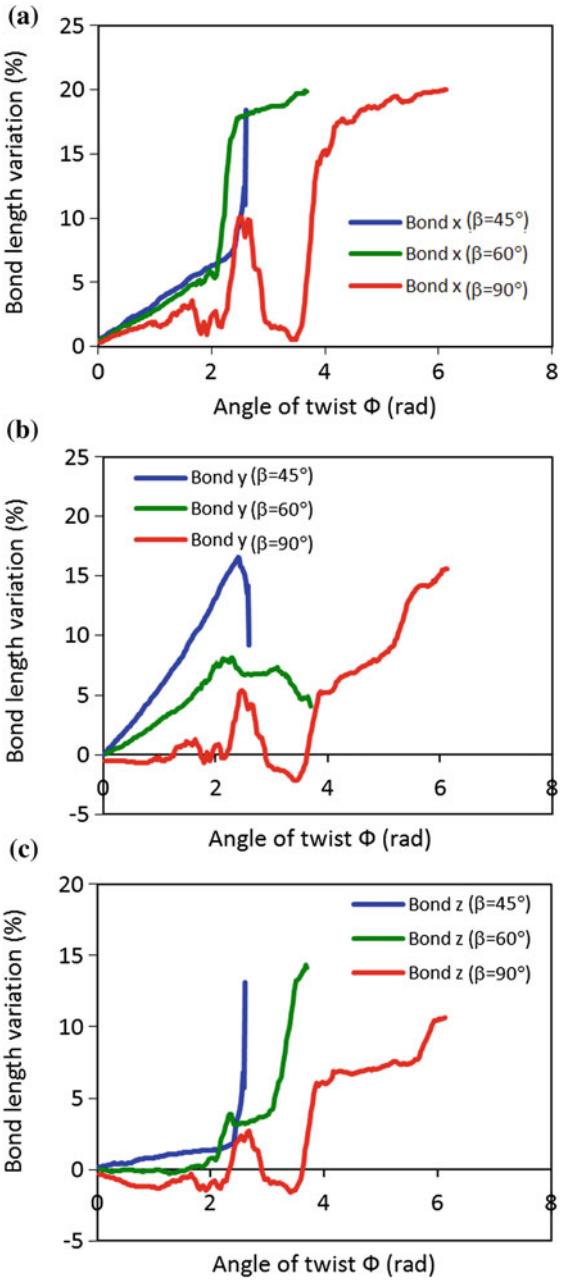

Fig. 14 CNT (8, 0): Variation, with the angle of twist ϕ (rad), of **a** bond x length variation, **b** bond y length variation, and **c** bond z length variation

For $\beta = 60°$, the bond length and angle amplitude variation curves do not exhibit a clear trend, but it is possible to discern four stages. Initially ($\phi < 2.0$ rad), there is a linear trend similar to that observed for $\beta = 45°$. For

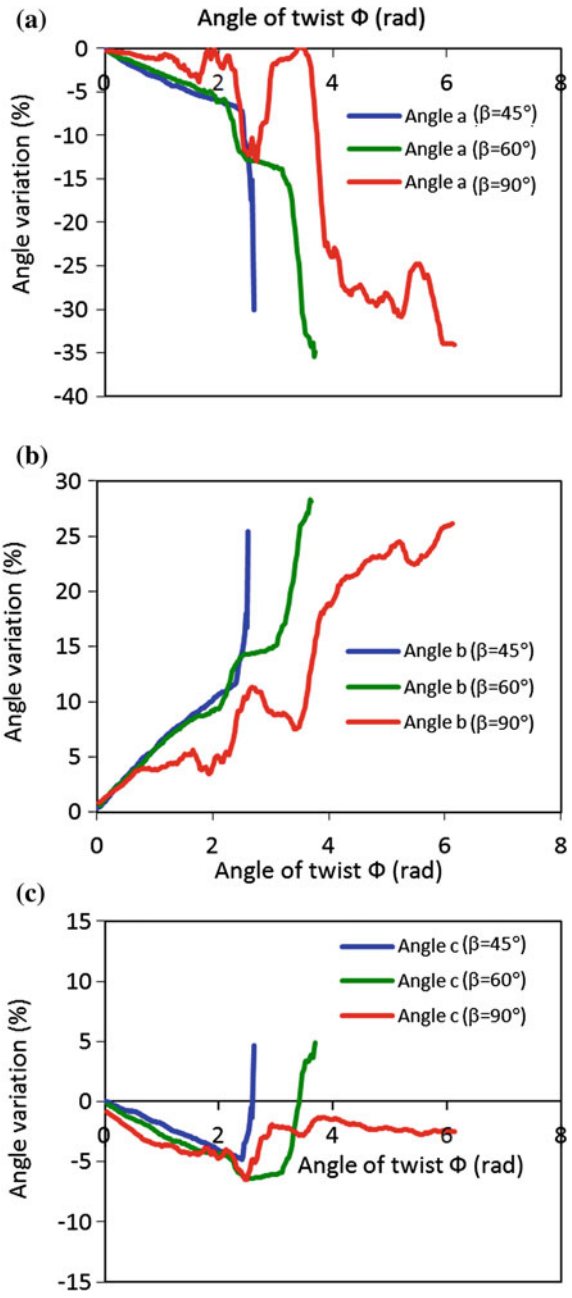

Fig. 15 CNT (8, 0): Variation, with the angle of twist ϕ (rad), of **a** angle a variation, **b** angle b variation, and **c** angle c variation

$2.0 < \phi < 2.33$ rad, the CNT buckles into a helix shape that oscillates about the CNT axis. The bonds **x** and **z** increase their length, especially bond **x** because it is oriented towards the stretching direction, while bond **y** maintains its length. Angles

a and **c** decrease their amplitude while angle **b** opens. These fluctuations reflect the consecutive reversible deformations of the lattice cell when the helix shape oscillates. These oscillations tend to redistribute and homogenize the bond and angle tensions throughout the CNT. This explains the huge increase of bond **x** length. These oscillations enable the load transfer from cell to cell in the axial directions. For $2.33 < \phi < 3.0$ rad, the helix shape oscillations almost stop. As twisting progresses beyond $\phi = 3.0$ rad, the helix shape is so twisted that the hexagonal cell distorts and CNT fails by the process depicted in Fig. 16. Deformation of the lattice cell consists mainly of the quick closing of angle **a** and opening of angles **b** and **c**. Notice that angle **c** was closing in previous stages, but this cell deformation increases the length of bond **z**, forcing angle **c** to open. The lengths of bonds **x** and **y** do not show much change because they were already stretched.

For $\beta = 90°$ (pure twisting), torsional buckling occurs very soon (at $\phi = 0.94$ rad) and, from then on, the helix shape oscillations alternate between high and low rotations. This gives rise to the red curves depicted in Figs. 14 and 15, in which the bond length and angle amplitude variations show a high scatter. For $\phi > 4.0$ rad, bond **x** increases its length almost 20 %, very close to the rupture length ($\sim$23 %), proving very good alignment with the stretching direction (CNT axis). The bonds **y** and **z** also increase length, as expected. A major difference to the combined twisting-stretching behaviour ($\beta = 45$ and 60°) is that the distortion of the hexagonal cell is not abrupt as it was for $\beta = 45$ and 60°. Angles show the same trend variations as before ($\beta = 60°$), but now are more gradual. The exception is that angle **c** no longer shows positive variation in this final stage before rupture (see Fig. 15c). This is a direct consequence of the length increase of bond **y**, which did not happen for $\beta = 60°$. This kinematic behaviour of bond

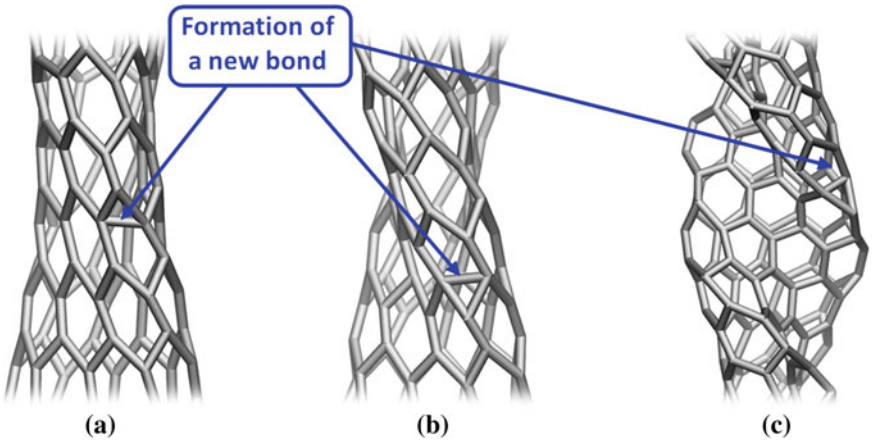

Fig. 16 (8, 0) CNT: views showing the formation of a new bond and beginning of the rupture process for **a** $\beta = 45°$, **b** $\beta = 60°$ and **c** $\beta = 90°$

y could be the result of the slow deformation of the hexagon cell, contrasting with the sudden deformation registered before ($\beta = 60°$).

For $\beta = 45$, 60 and 90°, Fig. 16 shows zoom-in views of new bond formation that consequently leads to CNT rupture. The distortion of hexagonal cell is clearly visible in Figs. 16a, b and c. It is also visible that cell deformation always occurs in the mostly bent and strained region of the buckled CNT. For $\beta = 45°$, it is interesting to notice that the closing of angle **a** is directly responsible for the creation of a new bond. However, for $\beta = 60$ and 90°, it is the closing of its symmetrical. Comparing Figs. 12 ((5, 5) CNT) and Fig. 16 ((8, 0) CNT), we conclude that the deformed shape of the cell is very similar.

Figure 17 depicts the variation of bond length and angle amplitude at rupture with β—recall that bond lengths and angle amplitudes are scaled to their initial values and they are the average value of the last 100 steps before rupture. From Fig. 17, it is seen that the influence of twisting-to-stretching rate ϕ/u (or β) on the kinematics of CNT rupture is deemed relevant. The bond **y** achieves the maximum

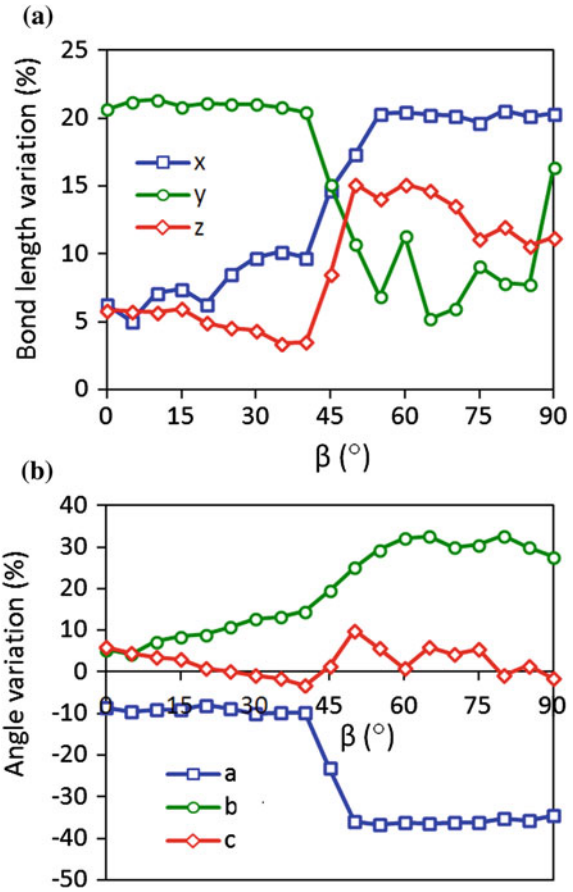

Fig. 17 CNT (8, 0): **a** bond length variation at rupture vs. β and **b** angle amplitude variation at rupture vs. β

elongation ($\sim$23 %) from $\beta = 0$ to 40° and the breaking of this bond initiates the CNT rupture. In this β range, bond **x** increases slightly its length because it becomes more align with the CNT axis due to the amount of twist. Oppositely, the bond **z** decreases its length. For the range $0° \leq \beta \leq 40°$, the amplitudes of the angles remain almost unchanged (Fig. 17b). For $45° \leq \beta \leq 90°$, there is a combination of angles typical of a distorted cell, with a sudden decline of angle **a** (even more closed) and increase of angle **b.** The combination of bond lengths also changes in this interval of β. From $\beta = 40$ to 50°, the lengths of bonds **x** and **z** increase while there is a major decline of the length of bond **y**. Although bond **x** achieves a maximum extension of 20 %, the rupture mechanism is not due to direct bond breaking but rather due to cell distortion. It is similar to the one described earlier for the (5, 5) CNT and $\beta \geq 20^{\circ}$.

5 Conclusion

This chapter presented a study on the kinematics of bonds and their influence on the collapse behaviour of armchair and zig-zag CNTs under combined stretching-twisting. MD simulations were used to achieve this goal and prescribed axial displacements (stretching) and twisting rotations (torsion) were imposed to both CNT ends (supports). The results were extensively analyzed, mainly in the form of (i) diagrams of energy at rupture versus the twisting-to-stretching rate and (ii) diagrams of interaction between the axial stretching displacement at rupture and the angle of twist at rupture. Then, a detailed study on the variation of bond length and angle amplitude with the imposed stretching and twisting deformations was shown. Firstly, the case of pure stretching was described as a reference. After that, the cases of combined twisting-stretching and pure twisting were dealt with separately for zig-zag (8, 0) CNT and armchair (5, 5) CNT.

From the remarks drawn before, we are now able to answer the question: why can (8, 0) CNT undergo more twisting compared with the (5, 5) CNT? The differences between the two CNTs (zig-zag and armchair) lie in the orientation of hexagonal cells, i.e. their chirality. With a meaningless amount of twist, the extension of the (5, 5) CNT is much higher (almost twice) than that of (8, 0) CNT because this CNT has only one bond (**y**) aligned with the axial direction while the armchair has two bonds (**y** and **z**) fairly aligned with the axial direction. For moderate to high twisting, the CNT rupture follows a different mechanism. Twisting deforms the matrix cells and brings carbon atoms into bond forming distances in order to promote the formation of new bonds and breaking more strained bonds. This mechanism relies on cell distortion. For the same twisting angle, the hexagonal cell of (5, 5) CNT deforms much more than that of (8, 0) CNT, meaning that rupture will occur sooner for the armchair CNT than for zig-zag one. Other factors may attenuate or contribute to cell deformation and may turn this dependence less clear, like load transfer, localized strain and rotational oscillations.

Acknowledgments The authors gratefully acknowledged the financial support given by FCT, in the context of the project "Modelling and Analysis of Nanostructures: Carbon Nanotubes and Nanocomposites" (PTDC/ECM/103490/2008).

References

Agrawal PM, Sudalayandi BS, Raff LM, Komanduri R (2008) Molecular dynamics (MD) simulations of the dependence of C–C bond lengths and bond angles on the tensile strain in single-wall carbon nanotubes (SWCNT). Comput Mater Sci 41:450–456

Arash B, Wang Q (2012) A review on the application of nonlocal elastic models in modeling of carbon nanotubes and graphenes. Comput Mater Sci 51(1):303–313

Bao WX, Zhu CC, Cui WZ (2004) Simulation of Young's modulus of single-walled carbon nanotubes by molecular dynamics. Phys B 352:156–163

Batra RC, Sears A (2007) Continuum models of multi-walled carbon nanotubes. Int J Solids Struct 44(22–23):7577–7596

Byrne EM, Letertre A, McCarthy MA, Curtin WA, Xia Z (2010) Optimizing load transfer in multiwall nanotubes through interwall coupling: theory and simulation. Acta Mater 58(19):6324–6333

Chang T (2007) Torsional behavior of chiral single-walled carbon nanotubes is loading direction dependent. Appl Phys Lett 90(20):201910

Faria B, Silvestre N, Canongia Lopes JN (2013a) Induced anisotropy of chiral carbon nanotubes under combined tension-twisting. Mech Mater 58:97–109

Faria B, Silvestre N, Canongia Lopes JN (2013b) Tension-twisting dependent kinematics of chiral CNTs. Compos Sci Technol 74:211–220

Fennimore AM, Yuzvinsky TD, Han WQ, Fuhrer MS, Cumings J, Zettl A (2003) Rotational actuators based on carbon nanotubes. Nature 424:408–410

Georgantzinos SK, Anifantis NK (2009) Vibration analysis of multi-walled carbon nanotubes using a spring-mass based finite element model. Comput Mater Sci 47(1):168–177

Hall AR, An L, Liu J, Vicci L, Falvo MR, Superfine R, Washburn S (2006) Experimental measurement of single-wall carbon nanotube torsional properties. Phys Rev Lett 96:256102

Hall AR, An L, Liu J, Vicci L, Falvo MR, Superfine R, Washburn S (2010) Erratum: Experimental measurement of single-wall carbon nanotube torsional properties [Phys Rev Lett 96 256102 (2006)]. Phys Rev Lett 105:069904

Hall AR, Paulson S, Cui T, Lu JP, Qin LC, Washburn S (2012) Torsional electromechanical systems based on carbon nanotubes. Rep Prog Phys 75(11):116501

Jeong BW, Lim JK, Sinnott SB (2007a) Tensile mechanical behavior of hollow and filled carbon nanotubes under tension or combined tension-torsion. Appl Phys Lett 90:023102

Jeong BW, Lim JK, Sinnott SB (2007b) Multiscale-failure criteria of carbon nanotube systems under biaxial tension-torsion. Nanotechnology 18:485715

Plimpton S (1995) Fast parallel algorithms for short-range molecular dynamics. J Comput Phys 117:1–19

Sears A, Batra RC (2004) Macroscopic properties of carbon nanotubes from molecular-mechanics simulations. Phys Rev B 69(23):235406

Shima H (2012) Buckling of carbon nanotubes: a state of the art review. Materials 5(1):47–84

Stuart SJ, Tutein AB, Harrison JA (2000) A reactive potential for hydrocarbons with intermolecular interactions. J Chem Phys 112:6472–6486

Sun J, Xu F, Sun LT (2012) In situ investigation of the mechanical properties of nanomaterials by transmission electron microscopy. Acta Mech Sin 28(6):1513–1527

Talukdar K, Mitra AK (2010) Influence of odd and even number of stone-wales defects on the fracture behaviour of an armchair single-walled carbon nanotube under axial and torsional strain. Mol Simul 36:409–417

Tserpes KI, Papanikos P, Tsirkas SA (2006) A progressive fracture model for carbon nanotubes. Compos B Eng 37(7–8):662–669

Wang Q, Liew KM (2008) Molecular mechanics modeling for properties of carbon nanotubes. J Appl Phys 103(4):046103

Wang CM, Zhang YY, Xiang Y, Reddy JN (2010) Recent studies on buckling of carbon nanotubes. Appl Mech Rev 63:030804

Wernik JM, Meguid SA (2010) Atomistic-based continuum modeling of the nonlinear behavior of carbon nanotubes. Acta Mech 212(1–2):167–179

Williams PA, Papadakis SJ, Patel AM, Falvo MR, Washburn S, Superfine R (2002) Torsional response and stiffening of individual multiwalled carbon nanotubes. Phys Rev Lett 89:255502

Xu YQ, Barnard A, McEuen PL (2009) Bending and twisting of suspended single-walled carbon nanotubes in solution. Nano Lett 9(4):1609–1614

Yakobson BI, Brabec CJ, Bernholc J (1996) Nanomechanics of carbon tubes: Instabilities beyond linear response. Phys Rev Lett 76:2511–2514

Zhao R, Luo CL (2011) Torsion-induced mechanical couplings of single-walled carbon nanotubes. Appl Phys Lett 99:231904